Article

Binding motifs for lanthanide-hydrides: a combined experimental and theoretical study of the MHx(H2)y species (M= La-Gd; x=2-4; y=0-6)

INFANTE, Ivan, *et al*.

Abstract

The results of a combined spectroscopic and computational study of lanthanide hydrides with the general formula MHx(H2)y, where M = La, Ce, Pr, Nd, Sm, Eu, and Gd, x = 1−4, and y = 0−6 are reported. To understand the nature of the dihydrogen complexes formed with lanthanide metal hydride molecules, we have first identified the binary MHx species formed in the ablation/deposition process and then analyzed the dihydrogen supercomplexes, MHx(H2)y. Our investigation shows that the trihydrides bind dihydrogen more weakly than the dihydrides and that the interaction between the central lanthanide and the H2 molecules occurs via a 6s electron transfer from the lanthanide to the H2 molecules. Evidence is also presented for the SmH and EuH diatomic molecules and the tetrahydride anions in solid hydrogen.

Reference

INFANTE, Ivan, *et al*. Binding motifs for lanthanide-hydrides: a combined experimental and theoretical study of the MHx(H2)y species (M= La-Gd; x=2-4; y=0-6). *The journal of physical chemistry. A*, 2009, vol. 113, no. 11, p. 2446-2455

DOI : 10.1021/jp8099658

Binding Motifs for Lanthanide Hydrides: A Combined Experimental and Theoretical Study of the $MH_x(H_2)_y$ Species (M = La−Gd; x = 1−4; y = 0−6)

Ivan Infante,[†] Laura Gagliardi,*[,†] Xuefeng Wang,[‡] and Lester Andrews*[,‡]

Department of Physical Chemistry, University of Geneva, 30 Quai Ernest Ansermet, CH-1211 Geneva, Switzerland, and Department of Chemistry, University of Virginia, Charlottesville, Virginia 22904-4319

Received: November 12, 2008; Revised Manuscript Received: December 23, 2008

The results of a combined spectroscopic and computational study of lanthanide hydrides with the general formula $MH_x(H_2)_y$, where M = La, Ce, Pr, Nd, Sm, Eu, and Gd, x = 1−4, and y = 0−6 are reported. To understand the nature of the dihydrogen complexes formed with lanthanide metal hydride molecules, we have first identified the binary MH_x species formed in the ablation/deposition process and then analyzed the dihydrogen supercomplexes, $MH_x(H_2)_y$. Our investigation shows that the trihydrides bind dihydrogen more weakly than the dihydrides and that the interaction between the central lanthanide and the H_2 molecules occurs via a 6s electron transfer from the lanthanide to the H_2 molecules. Evidence is also presented for the SmH and EuH diatomic molecules and the tetrahydride anions in solid hydrogen.

Introduction

An ideal chemical hydrogen storage material has a low molar weight, is inexpensive, has rapid kinetics for absorbing and desorbing H_2, and stores large quantities of hydrogen reversibly. Under these conditions, metal hydrides are of considerable interest because they, in principle, meet these requirements.[1] The challenge of finding suitable candidates also poses another question that is more pedagogical but equally fascinating: what is the maximum number of hydrogen atoms that a metal can bind?

Both theory and experiment play a major role in attempting to answer this question. In this contribution, we combine matrix infrared spectroscopy measurement and density functional calculations to achieve an understanding of the bonding between a metal and the hydrogen atoms.

The coordination of dihydrogen to metals has attracted considerable attention since the Kubas tungsten complexes were first discovered.[2−4] The metal hydride species, prepared with laser-ablated metal atoms and hydrogen, show two types of hydrogen−metal interactions, a direct σ metal hydride bond, in which the hydrogen shares its 1s electron with one of the available valence electrons of the metal, and a side-on type of bond, in which a dihydrogen molecule is "complexed" to the metal. The former is obviously the stronger kind and can give rise to four basic hydride species: MH, MH_2, MH_3, and MH_4. The latter bond will form a complex of type $MH_x(H_2)_y$ (x = 1−4; y = 0−6), in which the number of hydrogen atoms attached to it in the first shell, x, or hydrogen molecules in the second shell or side-bound ligand layer, y, will depend on the properties of the metal atom involved.

Infrared spectroscopic measurements for several metal compounds have been performed in noble gas matrices, and comprehensive works have been performed on lanthanide and group III metals.[5,6] However, performing these reactions in pure hydrogen will give a higher product yield and larger complexes and will provide further insight into the metal−hydrogen bond. Recently, we have reported the $WH_4(H_2)_4$ and $ThH_4(H_2)_4$ species using infrared spectroscopy and density functional theory (DFT) to identify the strongest vibrational frequencies and isotopic shifts of this complex.[7−9] The formation of $UH_4(H_2)_6$ has also been proposed,[10] which represents a record for the number of hydrogen atoms that can be bound to a metal.

In this investigation, we present the results of a systematic study of lanthanide hydrides with the general formula $MH_x(H_2)_y$, where M = La, Ce, Pr, Nd, Sm, Eu, and Gd, x = 1−4, and y = 0−6. Comparative calculations were also performed on the species in which the central metal, M, is Mo, W, and U. Earlier investigations from one of our laboratories focused on infrared spectra of these binary metal hydrides in solid argon.[11−13] Most germane to the present work is our early comprehensive report of lanthanide metal hydride molecules.[5] With the support of electronic structure calculations, we can better predict the nature of the metal−hydrogen interactions and which system presents the largest number of hydrogen molecules bonded to the central metal.

Computational and Experimental Methods

Quantum chemical calculations were performed using DFT. The TURBOMOLE package was employed.[14] Scalar relativistic effects were incorporated by employing on the lanthanide metal atoms the Stuttgart RSC Segmented/ECP basis set with 28 core electrons and contraction of (14s13p10d8f3g)/[10s8p5d4f3g] type.[15] A valence triple-ζ split valence basis set, TZVPP, was used on the hydrogen atoms. The gradient-corrected BP86 exchange correlation (xc) functional was employed. Some of the calculations were also repeated using the PBE[16] and PBE0 xc functionals.[17] Full geometry optimizations, frequency calculations, and assessment of the correct ground-state spin multiplicity were performed for all species. Basis set superposition error (BSSE) corrections were included using the counterpoise method. Zero-point energy corrections (ZPE) were also computed.

We have studied the interaction between the hydrogen atoms and the metal by classifying the energy of the MH_x systems in

* Corresponding authors. E-mail: laura.gagliardi@chiphy.unige.ch (L.G.), lsa@Virginia.edu (L.A.).
[†] University of Geneva and University of Minnesota.
[‡] University of Virginia.

10.1021/jp8099658 CCC: $40.75

a series of contributions. The bonding energy, ΔE_{bond}, between two fragments is expressed as the sum of two terms: one destabilizing term called strain energy or preparation energy, ΔE_{strain} (the two expressions will be used as synonyms in the following), and one stabilizing term called interaction energy, ΔE_{int} ($\Delta E_{bond} = \Delta E_{strain} + \Delta E_{int}$). ΔE_{strain} is associated with the deformation of the individual fragments when they form the supersystem. This contribution is always positive, and its magnitude depends on the rigidity and reorganization of each fragment. ΔE_{int} is the effective interaction between the deformed fragments. This procedure has shown to be very informative for similar systems.[18−20] To analyze the charge transfer between the metal and the hydrogen moieties, we used the natural population charges as implemented in TURBOMOLE.

The experiment for reactions of laser-ablated lanthanide metal atoms with hydrogen molecules during condensation at 4 K has been previously described in detail.[21] The Nd/YAG laser fundamental (1064 nm, 10 Hz repetition rate with 10 ns pulse width) was focused onto a rotating metal target (Johnson−Matthey). The laser energy was varied from 1 to 10 mJ/pulse. Laser-ablated lanthanide metal atoms were codeposited with 3 to 4 mmol of normal or *para*-hydrogen[22,23] molecules onto a 4 K CsI cryogenic window for 30 min using a Sumitomo Heavy Industries Model RDK-205D cryocooler. Hydrogen (Matheson), D_2, and HD (Cambridge Isotopic Laboratories) were used in different experiments. FTIR spectra were recorded at 0.5 cm^{-1} resolution on a Nicolet 750 apparatus with 0.1 cm^{-1} accuracy using a HgCdTe range B detector. Matrix samples were annealed at different temperatures, and selected samples were subjected to broadband photolysis by a medium-pressure mercury arc lamp (Philips, 175W) with the outer globe removed.

Results and Discussion

DFT-based calculations were initially performed to optimize the structures of all possible $MH_x(H_2)_y$ species and to determine the interaction energy of the classical MH_x with several dihydrogen molecules. Solid hydrogen matrix infrared spectroscopy was then used to provide "matrix shifts" in the guest molecule frequencies and uncertainties in the number of complexing dihydrogen ligands associated with a particular binary lanthanide metal hydride core molecule. With the interplay of the two approaches, we were able to provide new spectroscopic and computational information for such difficult metal hydride systems and to find a consistent model to explain the properties of these new dihydrogen complexes.

Structure and Energetics. The metal−hydrogen bond distances for several metal hydrides are reported in Table 1. For a given structure, two kinds of M−H bonds were considered, namely, $M-H^1$ for the σ-bonded hydrogen atoms (the classical hydrides) and $M-H^2$ for the bond with a H_2 molecule (a dihydrogen ligand). The values reported in Table 1 have been averaged over all possible $M-H^1$ and $M-H^2$ bond distances for a particular $MH_x(H_2)_y$ species [$x = 2, 3, 4$; $y = 0-6$]. In Table 2, we report the spin multiplicities for the electronic ground state of all of the species reported in Table 1.

We decided to proceed in a multistep way by adding one hydrogen molecule at a time to the MH_x classical hydride and allowing a full geometry optimization for each cluster. This approach should, in principle, be representative of what happens experimentally when the hydrogen molecules bond one after the other to the MH_x molecules produced in the laser-ablated and excited metal atom reactions. Computationally, we compare the total energy (including ZPE) of the $MH_4(H_2)_y$ and $MH_2(H_2)_{y+1}$ clusters to decide which of the two types is more stable and is thus likely to be formed in the matrix. We assume that both types of clusters have the same kinetics of absorbing H_2 molecules. Even if most lanthanides are strongly trivalent, for the $MH_3(H_2)_y$ species, such energy comparisons are more difficult because of the different stoichiometry. However, excess energy is available in the laser-ablation process, and the MH_3 species can be formed through the reaction of MH and H_2 molecules or H atoms and MH_2 molecules.

The calculations indicate that with the exception of cerium, most of the lanthanides preferentially form the $MH_2(H_2)_{y+1}$ species rather than the $MH_4(H_2)_y$ compounds, especially when y is equal to 1, 2, and 3. Some compounds, like $MH_4(H_2)_4$ (M = Pr, Nd), have been successfully optimized, and they present all real frequencies. However, they are less likely to form experimentally. This interpretation finds confirmation in Table

TABLE 1: Typical Bond Metal Hydride and Metal Dihydrogen Distances (Å) for Various Ground-State Species of $MH_2(H_2)_y$, $MH_3(H_2)_y$, and $MH_4(H_2)_y$ Computed at DFT/BP86/TZVPP Level of Theory[a]

MH_2	La	Ce	Pr	Nd	Sm	Eu	Gd
$y = 0$	2.14	2.07	2.09	2.10	2.11	2.11	2.04
$y = 1$	2.11	2.08	2.10	2.11	2.11	2.11	2.05
	2.38	2.31	2.37	2.44	2.57	2.67	2.45
$y = 2$	2.13	2.08	2.10	2.09	2.12	2.12	2.05
	2.46	2.42	2.49	2.53	2.50	2.47	2.49
$y = 3$	2.14	2.08	2.09	2.12	2.13	2.13	2.06
	2.47	2.42	2.43	2.47	2.46	2.43	2.55
$y = 4$	2.14	2.09	2.11	2.13	2.13	2.13	
	2.46	2.43	2.41	2.45	2.46	2.48	
$y = 5$	2.15	2.09	2.12	2.12	2.13	2.14	
	2.48	2.42	2.44	2.43	2.48	2.48	
$y = 6$	2.15	2.10	2.11	2.12	2.13	2.15	
	2.49	2.43	2.44	2.45	2.47	2.48	
MH_3	La	Ce	Pr	Nd	Sm	Eu	Gd
$y = 0$	2.12	2.06	2.05	2.06	2.09	2.10	2.01
$y = 1$	2.13	2.06	2.05	2.04	2.07	2.10	2.03
	2.40	2.33	2.29	2.26	2.25	2.32	2.45
$y = 2$	2.13	2.07	2.05	2.04	2.06	2.11	2.03
	2.42	2.34	2.31	2.29	2.30	2.27	2.46
$y = 3$	2.14	2.07	2.06	2.04	2.07	2.12	2.04
	2.43	2.36	2.34	2.32	2.34	2.34	2.47
$y = 4$	2.14	2.08	2.06	2.05	2.07	2.12	2.04
	2.45	2.40	2.37	2.36	2.39	2.38	2.54
$y = 5$	2.16	2.09	2.07	2.06	2.07	2.12	
	2.48	2.42	2.40	2.37	2.40	2.41	
$y = 6$	2.16	2.10	2.08	2.07	2.08	2.12	
	2.50	2.45	2.42	2.40	2.39	2.43	
MH_4	Cr	Mo	W	Nd	U		
$y = 1$	1.64	1.64	1.67	2.11	2.01		
	1.95	1.69	1.71	2.44	2.19		
	as $CrH_2(H_2)$			as $NdH_2(H_2)$			
$y = 2$	1.66	1.66	1.69	2.11	2.01		
	1.91	as MoH_6	as WH_6	2.44	2.24		
	as $CrH_2(H_2)_2$			as $NdH_2(H_2)$			
$y = 3$	1.61	1.71	1.72	2.11	2.01		
	1.71	1.81	1.86	2.44	2.27		
	as $CrH_2(H_2)_3$			as $NdH_2(H_2)_2$			
$y = 4$	1.67	1.72	1.74	2.13	2.02		
	as $Cr(H_2)_5$	1.83	1.85	2.45	2.31		
				as $NdH_2(H_2)_2$			
$y = 5$	1.67			2.12	2.02		
	as $Cr(H_2)_6$			2.43	2.32		
				as $NdH_2(H_2)_2$			
$y = 6$				2.12	2.03		
				2.45	2.34		
				as $NdH_2(H_2)_2$			

[a] In the case of Cr, more than one H_2 molecule is attached to the metal, and thus the supercomplex transforms first into $CrH_2(H_2)_y$ for $y < 3$ and then into $Cr(H_2)_y$. As for the Nd species, the $NdH_4(H_2)_y$ is always less stable than its $NdH_2(H_2)_{y+1}$ isomer and in most cases does not form a stable minimum (i.e., no imaginary frequencies) or is found at much higher energies, hence we do not consider it here.

TABLE 2: Spin Multiplicities for Each of the Electronic Ground-State Species Optimized At DFT/BP86/TZVPP Level of Theory[a]

	La	Ce	Pr	Nd	Sm	Eu	Gd
MH	singlet	doublet	triplet	sextet	octet	nonet	octet
MH_2	doublet	triplet	quartet	quintet	septet	octet	nonet
MH_3	singlet	doublet	triplet	quartet	sextet	septet	octet
MH_4	doublet	singlet	doublet	triplet	quintet	sextet	nonet
MH_4^-	singlet	doublet	triplet	quartet	sextet	septet	octet
$MH_2(H_2)_y$ [y = 1,..., 6]	doublet	triplet	quartet	quintet	septet	octet	nonet
$MH_3(H_2)_y$ [y = 1,..., 6]	singlet	doublet	triplet	quartet	sextet	septet	octet
	Cr	Mo	W	Nd	U		
MH_2	quintet	quintet	quintet	quintet	quintet		
MH_4	quintet as $CrH_2(H_2)$	triplet	triplet	triplet	triplet		
$MH_4(H_2)$	quintet as $CrH_2(H_2)_2$	singlet as MoH_6	singlet as WH_6	quintet as $MH_2(H_2)_2$	triplet		
$MH_4(H_2)_2$	quintet as $CrH_2(H_2)_3$	singlet	singlet	quintet as $MH_2(H_2)_3$	triplet		
$MH_4(H_2)_3$	singlet as $Cr(H_2)_5$	singlet	singlet	quintet as $MH_2(H_2)_4$	triplet		
$MH_4(H_2)_4$	singlet as $Cr(H_2)_6$	singlet	singlet	quintet as $MH_2(H_2)_5$	triplet		

[a] All of the relevant structures are presented. For the group VI elements, we report only the species with an even number of hydrogen atoms because the oddly numbered species are not met in the experimental conditions.

TABLE 3: Energy Differences (kcal/mol) between MH_4 and Other Isomeric Species with M = La, Ce, Pr, Nd, Sm, Eu, Gd, Cr, Mo, W, and U computed at DFT/BP86/TZVPP Level of Theory[a]

	La	Ce	Pr	Nd	Sm	Eu	Gd
$E[MH_4]-E[MH_2(H_2)]$	31.5	12.2	35.5	46.9	56.8	64.5	3.3
	(26.5)	(9.6)	(31.7)	(42.9)	(52.4)	(60.4)	(3.3)
$E[MH_4]-E[M(H_2)_2]$	15.7	−6.9	19.0	29.9	42.9	71.9	−15.9
	(8.6)	(−10.9)	(15.2)	(23.9)	(36.5)	(68.1)	(−17.6)
$E[MH_4]-E[MH_2]-E[H_2]$	18.6	7.6	32.1	43.2	54.3	63.1	0.4
	(17.1)	(−8.3)	(31.5)	(42.1)	(52.6)	(61.3)	(3.5)
	Cr	Mo	W	Nd	U		
$E[MH_4]-E[MH_2(H_2)]$	16.4	−13.1	−24.6	46.9	−9.5		
	(15.6)	(−13.3)	(−24.7)	(42.9)	(−10.9)		
$E[MH_4]-E[M(H_2)_2]$	2.3	−22.6	−44.4	29.9	−31.1		
	(1.3)	(−23.8)	(−44.0)	(23.9)	(−34.2)		
$E[MH_4]-E[MH_2]-E[H_2]$	10.8	−19.5	−32.6	43.2	−12.6		
	(13.3)	(−16.7)	(−29.7)	(42.1)	(−11.4)		

[a] A negative value means that the MH_4 is the most stable conformer. In parentheses, values including the zero-point energy correction are reported.

3, where we compared the stability (including ZPE) of MH_4 to that of $MH_2(H_2)$ and $M(H_2)_2$. It is evident that the MH_4 fragment is thermodynamically less stable than, for example, $MH_2(H_2)$. The only exception is represented by cerium, for which the energy difference between MH_4 and $MH_2(H_2)$ is not very large (about 10 kcal/mol), and we were able to compute all types of complexes. This result is also confirmed by a previous laser ablation experiment using argon as the trapping material, where traces of CeH_4 have been identified.[5]

In the middle of the row, the gadolinium classical hydride GdH_2 binds only weakly to any H_2 molecule. Without the inclusion of the ZPE, the formation of the supercomplexes is slightly favorable, whereas with ZPE, the reactants (i.e., the separate fragments) are more stable of about 1 to 3 kcal/mol. However, the latter result may very well be a flaw of the calculations because the error in the DFT interaction energies can be larger than these small values. Therefore, because experimentally weak bands of supercomplexes of gadolinum are visible, we assume that the interaction exists, even if it is very small.

For samarium and europium, the formation of $MH_2(H_2)_x$ with $x = 1, 2, 3$ is also hindered from a computational standpoint, and this would suggest that the heavier lanthanides Sm, Eu, and Gd would not form any supermolecular reaction products with an even number of hydrogen atoms. However, as in the case of Gd, the presence of weak bands of supercomplexes in the spectra suggests the formation of a bonding interaction, even though it is weak.

The MH_3 fragments are also more favorable to the complexation with H_2 molecules in the case of M = Sm, Eu, and Gd, thus indicating that these lanthanide species could also form stable agglomerates.

For the compounds of group VI elements (Cr, Mo, W) and uranium, the situation is different. Chromium preferentially forms the $CrH_2(H_2)_y$ systems with y up to 3. For $y > 3$, the $Cr(H_2)_{y+1}$ clusters are more stable than the $CrH_2(H_2)_y$ clusters. An inspection of Table 3 shows that Mo, W, and U largely favor the MH_4 species (with respect to $MH_2(H_2)$, $M(H_2)_2$), and for these elements, we decided to study mainly the $MH_4(H_2)_y$ supermolecules because of the clear experimental evidence of the dominating presence of these species in the vibrational spectra.[11−13]

In Figure 1a,b, we report the energy difference $E[MH_2(H_2)_y] - E[MH_2] - yE[H_2]$ versus the number, y, of H_2 molecules

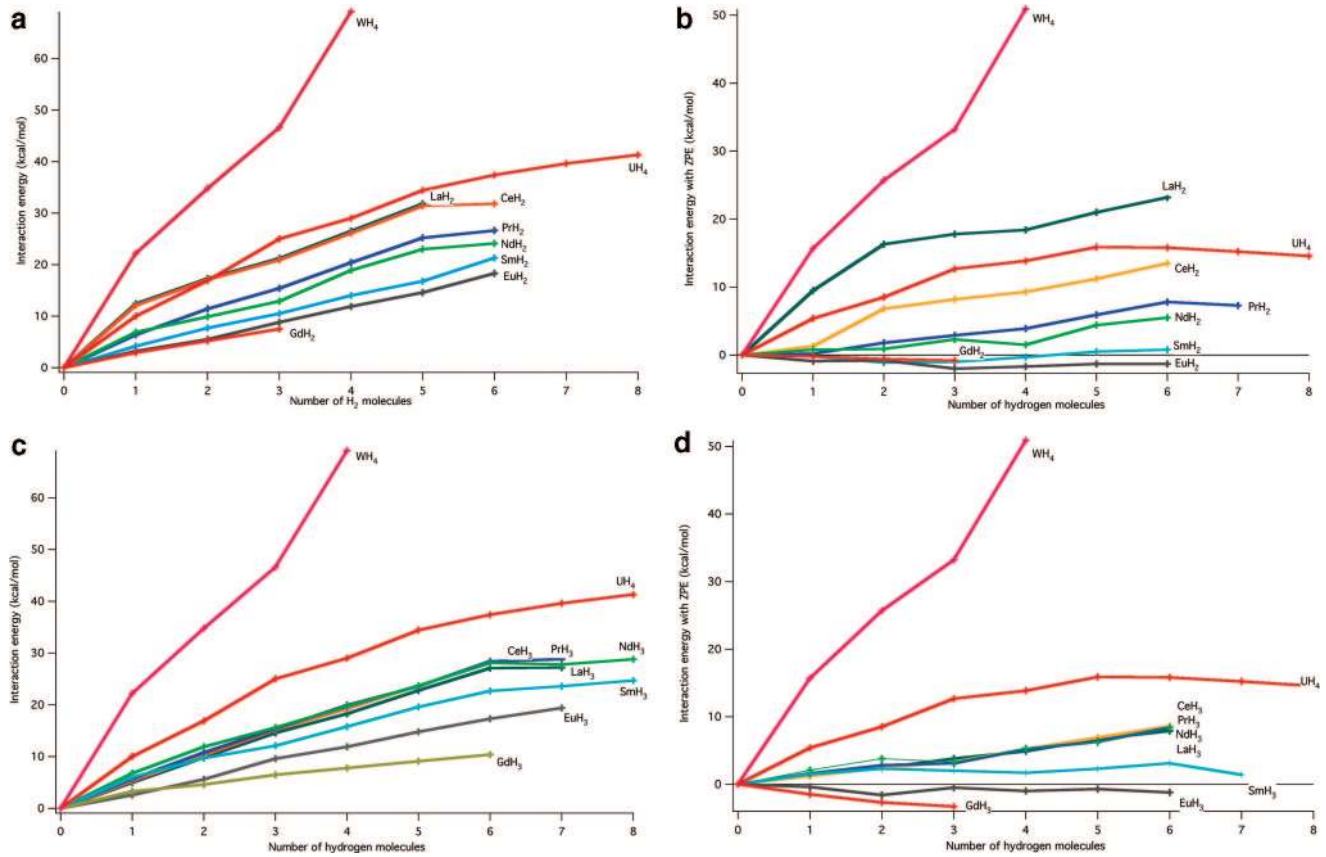

Figure 1. Energy difference $E[MH_x(H_2)_y] - E[MH_x] - yE[H_2]$ [$x = 2, 3$] versus the number, y, of H_2 molecules (a,c) without ZPE corrections and (b,d) with the ZPE correction. All values were computed at DFT/BP86/TZVPP level of theory. The BSSE effect, around 1 to 2 kcal/mol, is not included.

without and with the ZPE correction, respectively. In Figure 1c,d we report the energy difference $E[MH_3(H_2)_y] - E[MH_3] - yE[H_2]$ versus the number, y, of H_2 molecules without and with the ZPE correction, respectively. The stability of the W and U clusters is also reported for comparison. Because of the choice of a large basis set, the BSSE effects (benchmarked only on selected species) on the energy differences are reasonably small, around 1 to 2 kcal/mol. This value is smaller than the energy gain obtained by adding H_2 for small values of y, but it becomes of the same order of magnitude when y is larger than 6. This suggests that the energy gain for $y > 6$ shown in Figure 1a,c may not actually occur. Furthermore, Figure 1b,d, where the ZPE corrections have been added, show that the interaction energies are drastically reduced for all elements and that some species such as $SmH_2(H_2)_x$ and $EuH_2(H_2)_x$ have negative values, indicating a disproportioning of the supercomplex $MH_2(H_2)_x$ to the isolated fragments. A similar pattern is found for the $MH_3(H_2)_x$ species. However, these negative values are of the same order of magnitude as the approximations used in the calculations. Indeed, we have observed SmH_2 and EuH_2 in solid hydrogen, but the interaction with extra H_2 could be weak, as the DFT results suggest. Therefore, we can just obtain these molecules trapped in solid hydrogen without forming stable complexes with more H_2 molecules.

Regarding the group VI series and uranium, the striking feature remains the much larger stabilization energy of $MoH_4(H_2)_y$ and $WH_4(H_2)_y$ upon the addition of H_2 molecules. For $y = 4$, which is the maximum y (number of H_2 molecules) reachable for these complexes, the interaction energy with the H_2 molecules is at least three times larger than that for the lanthanide atoms. UH_4 has a stabilization energy of about 25 kcal/mol, which is larger than that in the NdH_4 case but smaller compared with the 65 kcal/mol of WH_4. Despite the smaller interaction energy, UH_4 has enough space to accommodate up to five or six H_2 molecules.

Summarizing our calculations, among all of the possible lanthanide MH_x classical hydrides, the only ones that may form stable supercomplexes of $MH_x(H_2)_y$ type are La, Ce, Pr, and Nd. Among these, only Cerium shows the formation of tetravalent $CeH_4(H_2)_y$ hydrides, whereas the others can form only divalent $MH_2(H_2)_y$ or trivalent $MH_3(H_2)_y$ hydrides. All elements could form stable basic MH_x (with $x = 2, 3, 4$) components with no H_2 molecules attached. Only weak interactions can be obtained for Sm, Eu, and Gd, but they are strong enough to be identified as weak bands in the experimental spectra. For elements of group VI, chromium mainly forms aggregates of $CrH_2(H_2)_y$ type or $Cr(H_2)_{y+1}$ for $y > 3$, whereas Mo, W, and U form supercomplexes of $MH_4(H_2)_y$ type only. Among all of these combinations of supercomplexes, the maximum number of hydrogen atoms that can be attached to a metal is 14 to 15, a value achieved by La, Ce, Pr, Nd, and U. Uranium can probably also form the species $UH_4(H_2)_6$ with 16 hydrogens in all. In the Ln compounds, as in the group VI, U, and Nd compounds, the H−H bond distance of the H_2 moieties significantly elongates (about 0.80 Å, see the Supporting Information). In Figure 2a,b, the structures for $MH_4(H_2)_4$ in which the metal is a lanthanide atom or a group VI atom, such as tungsten, are reported, respectively.

Infrared Spectra. Infrared spectra were recorded from samples prepared by codepositing laser-ablated early lanthanide metal atoms and normal hydrogen at 4 K. These spectra contain bands due to solid hydrogen and the trapped hydride anion as

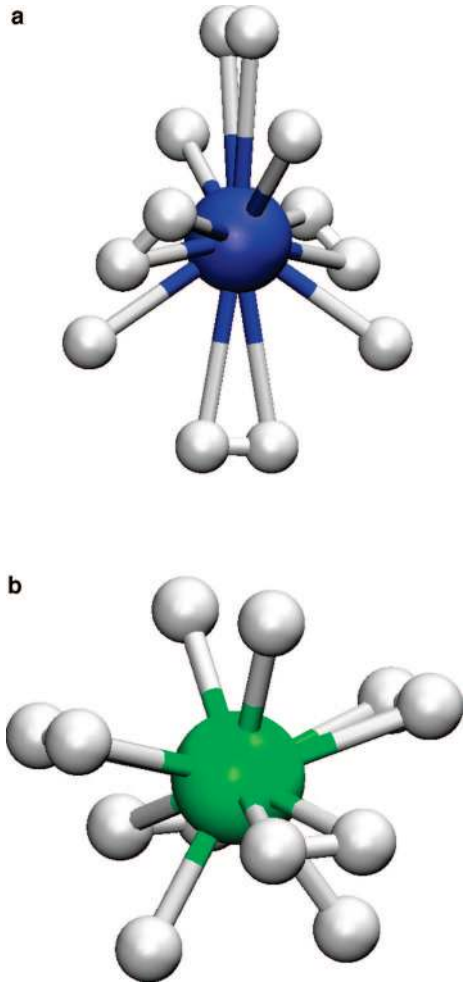

Figure 2. Structures for $MH_4(H_2)_4$ in which the metal is (a) a lanthanide atom or (b) a group VI atom, such as tungsten. A different type of bonding occurs with the peripheral H_2 molecules.

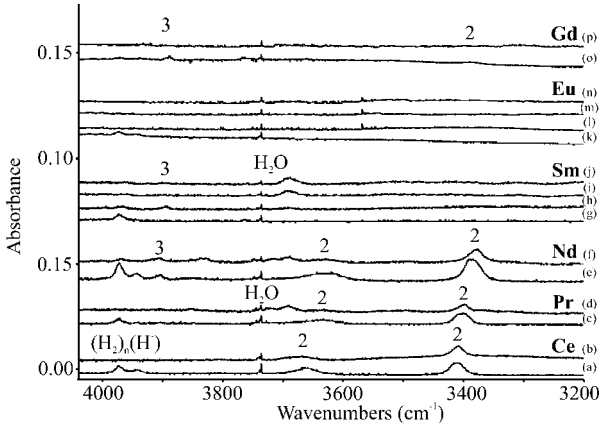

Figure 3. Infrared spectra for the products of reaction of early lanthanide metal atoms with dihydrogen during co-condensation at 4 K. (a) Ce codeposition, (b) after >290 nm irradiation; (c) Pr codeposition, (d) after 240−380 nm irradiation; (e) Nd codeposition, (f) after 240−380 nm irradiation; (g) Sm codeposition, (h) after >470 nm irradiation, (i) after 240−380 nm irradiation, and (j) after >530 nm irradiation; (k) Eu codeposition, (l) after >470 nm irradiation, (m) after >380 nm irradiation, and (n) after 240−380 nm irradiation; and (o) Gd codeposition, (p) after >320 nm irradiation.

it perturbs the surrounding dihydrogen ligands.[24] Infrared spectra of the important new absorptions are shown in Figures 3 and 4 for the H−H and Ln−H stretching regions. To understand the dihydrogen complexes formed with lanthanide metal hydride

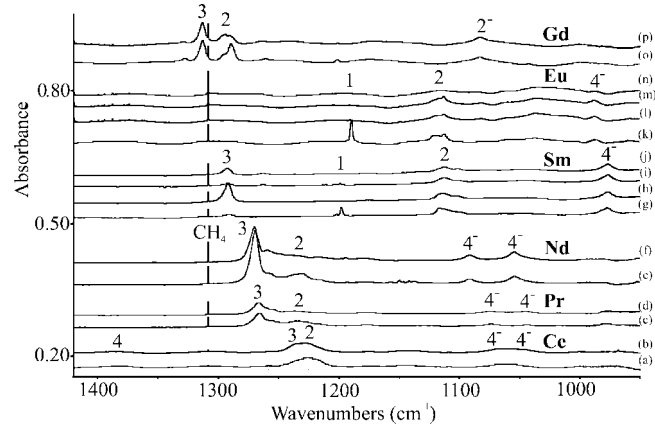

Figure 4. Infrared spectra for the products of reaction of early lanthanide metal atoms with dihydrogen during co-condensation at 4 K. (a) Ce codeposition, (b) after >290 nm irradiation; (c) Pr codeposition, (d) after 240−380 nm irradiation; (e) Nd codeposition, (f) after 240−380 nm irradiation; (g) Sm codeposition, (h) after >470 nm irradiation, (i) after 240−380 nm irradiation, and (j) after >530 nm irradiation; (k) Eu codeposition, (l) after >470 nm irradiation, (m) after >380 nm irradiation, and (n) after 240−380 nm irradiation; and (o) Gd codeposition, (p) after >320 nm irradiation.

molecules, we first need to identify the binary LnH_x molecule formed in the ablation/deposition process, which becomes the core in the dihydrogen supercomplex. To this end, we compare spectra in the Ln−H stretching region where product bands are labeled with small numbers (x), which indicate the number of classical hydrides on the metal center, that is, LnH_x. This LnH_x molecule forms the core of a larger dihydrogen complex, $LnH_x(H_2)_y$, which is the subject of our investigation.

Notice first that there is a single band labeled 4 (Figure 4a). In the case of Ce, we believe that this weak 1381 cm^{-1} absorption is due to $CeH_4(H_2)_y$ because isolated CeH_4 in solid argon was assigned at 1442 cm^{-1}.[5] Next, realize that the spectra are dominated by bands labeled 3 with the notable exception of spectra recorded after Eu reactions (k−n). These bands labeled 3 correlate reasonably well with the calculated position of the strongest absorptions for the corresponding $LnH_3(H_2)_y$ complexes, including the failure to converge a stable EuH_3 molecule. The LnH + H_2 reaction energies provide some measure of how favorable the LnH_3 product is in these experiments, and we note that EuH_3 has the highest endothermic value (+29 kcal/mol) and CeH_3 is the most exothermic (−24 kcal/mol). It is important that we have mixed isotopic spectra from experiments with pure HD that convincingly identify the gadolinium dihydride and trihydride core molecules (Figure 5). First, the GdH_2 absorptions at 1327.2 and 1289.1 cm^{-1} are near our computed 1330 and 1268 cm^{-1} values for the GdH_2 molecule in the nonet ground state but lower than the solid argon values of 1399.0 and 1359.3 cm^{-1}.[5] The single intermediate band at 1307.0 cm^{-1} is then due to GdHD for this core molecule with two equivalent H(D) atoms. Notice that some GdH_2 is also observed in solid HD slightly lower at 1324.9 and 1285.8 cm^{-1}, which in this case arises because of isotopic exchange leaving behind a D_2 ligand, $GdH_2(D_2)$. Similar isotopic rearrangements between classical and nonclassical hydride positions have been observed in other such complexes.[6,8] Clearly, a weak dihydrogen complex is formed with GdH_2 in solid hydrogen, but our calculations find that the binding of H_2 to GdH_2 is very weak, and we cannot determine the number of such H_2 ligands. We do, however, associate the 3385 cm^{-1} band and the much stronger deuterium counterpart at 2441 cm^{-1} (H/D ratio 1.3867) with the strongest of such H−H stretching modes of this

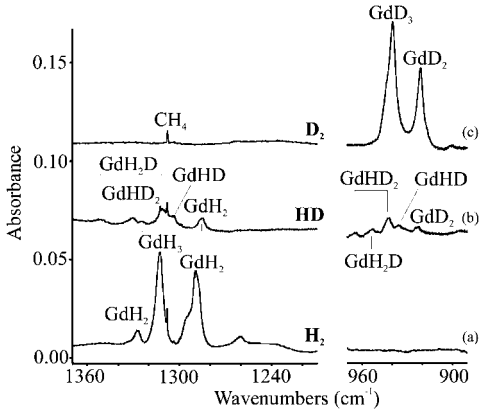

Figure 5. Infrared spectra for the major Gd atom reaction products with isotopic molecular hydrogen samples during codeposition at 4 K. (a) H_2, (b) HD, and (c) D_2. The labels identify the core isotopic molecules in larger complexes. In the HD experiment, the $GdH_2(D_2)$ and $GdD_2(H_2)$ complexes are implicated through isotopic positional exchange.

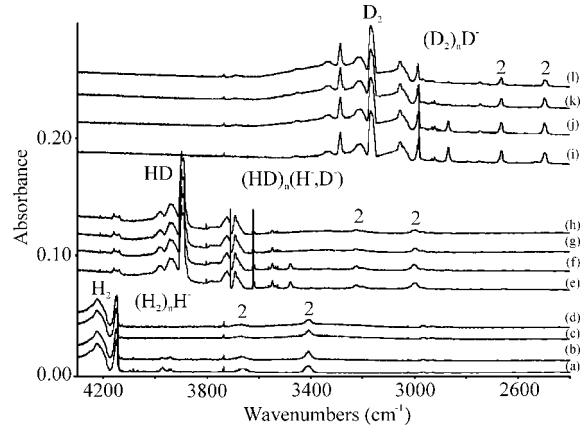

Figure 6. Infrared spectra for the Ce atom reaction product with isotopic molecular hydrogens. (a) Co deposition with H_2, (b) after >320 nm irradiation, (c) after >290 nm irradiation, and (d) after annealing to 6.5 K; (e) Codeposition with HD, (f) after >470 nm irradiation, (g) after >290 nm irradiation, and (h) after annealing to 8 K; and (i) Codeposition with D_2, (j) after 630 nm irradiation, (k) after >290 nm irradiation, and (l) after >220 nm irradiation.

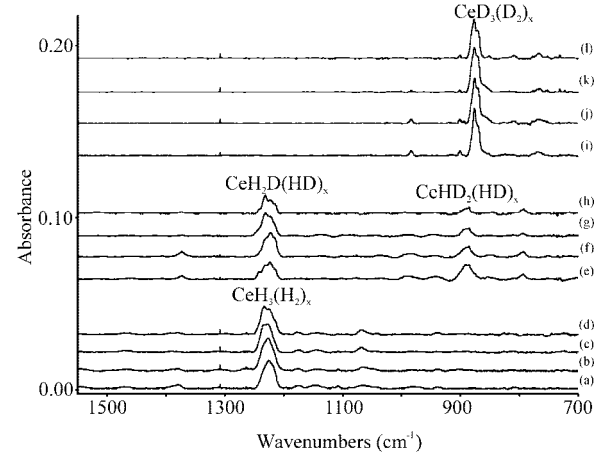

Figure 7. Infrared spectra for the Ce atom reaction product with isotopic molecular hydrogens. (a) Co deposition with H_2, (b) after >320 nm irradiation, (c) after >290 nm irradiation, and (d) after annealing to 6.5 K; (e) Codeposition with HD, (f) after >470 nm irradiation, (g) after >290 nm irradiation, and (h) after annealing to 8 K; and (i) Codeposition with D_2, (j) after 630 nm irradiation, (k) after >290 nm irradiation, and (l) after >220 nm irradiation.

$GdH_2(HH)_x$ complex. Second, the strong GdH_3 antisymmetric Gd−H stretching mode at 1312.9 cm^{-1} is near our calculated 1296 cm^{-1} value, which is satisfactory considering all of the approximations involved. The GdH_2D isotopic modification will then have an antisymmetric GdH_2 mode near that of GdH_3 (the 1311.3 cm^{-1} band in solid HD is identified accordingly) and a higher-frequency symmetric GdH_2 stretching counterpart (because the weaker nondegenerate mode for GdH_3 is computed to be higher than the degenerate mode), and the 1351.8 cm^{-1} band fits. The nearly median band at 1330.9 cm^{-1} is then due to the single Gd−H stretching mode of $GdHD_2$. In solid D_2, the GdD_2 molecule is observed at 921.5 cm^{-1}, and the GdHD(HD) band is observed at 936.2 cm^{-1} in solid HD. The degenerate mode of GdD_3 is at 939.9 cm^{-1} in solid D_2, and the antisymmetric Gd−D mode of $GdHD_2$ is at 943.2 cm^{-1} with the symmetric counterpart at 964.8 cm^{-1} in solid HD. The intermediate band at 953.8 cm^{-1} is the Gd−D stretching mode of GdH_2D. Therefore, in solid HD, we observed three stretching modes for each of the two mixed isotopic core molecules GdH_2D and $GdHD_2$, which confirms their identification as trihydride core molecules. Isotopic substitution, isotopic frequency calculations, and previous work[5] support this conclusive isotopic identification of the trihydride species.

Notice next that the 3 bands increase on light irradiation, whereas the 2 bands decrease. This enables us to associate weak H−H stretching modes near 3900 cm^{-1} with the trihydride complex and stronger such bands in the 3400−3600 cm^{-1} region with the dihydride complexes. We note that the H/D ratios of these two distinctly different H−H stretching absorptions are also different, with the higher bands near 1.389 and the lower bands near 1.375 and 1.365 for the two in Figure 3a. The more strongly bound and more red-shifted H−H stretching modes are often more anharmonic, as indicated by the lower H/D isotopic frequency ratios. This may suggest that LnH_3 binds H_2 more weakly than LnH_2, even if the energy differences are small.

The 1233.7 cm^{-1} peak in the Ce experiment increases upon irradiation and is assigned to the $CeH_3(H_2)_y$ complex, which is in accord with the present computations. The 1224.6 cm^{-1} peak that decreases on irradiation is then attributed to the $CeH_2(H_2)_y$ complex, which follows our calculations and the previous 1282 cm^{-1} solid argon identification.[5] We repeated these argon matrix experiments including HD and D_2 substitution and reaffirm the CeH_2 assignment but not the CeH_3 assignment.[5] The 3662 and 3409 cm^{-1} bands (labeled 2 in Figure 3) have HD and D_2 counterparts at 3222 and 2998 cm^{-1} and at 2664 and 2497 cm^{-1} in Figure 6 (H/D ratios 1.3746 and 1.3652). These are clearly due to H_2 (HD or D_2) ligand stretching modes. Figure 7 shows the Ce−H and Ce−D stretching regions of the spectra. Figure S1 in the Supporting Information compares spectra for the Ce reaction with *para*-hydrogen and *ortho*-deuterium. Finally, the two 1265.6 and 1232.9 cm^{-1} bands using Pr have the analogous $PrH_3(HH)_y$ and $PrH_2(HH)_y$ assignments following the 1286 cm^{-1} attribution to PrH_2 in solid argon.

The strong 1269.5 cm^{-1} band observed here for NdH_3 in solid hydrogen is in line with the present calculation of strong bands at 1310 and 1324 cm^{-1} for this molecule, and both show that the earlier 1150 cm^{-1} assignment[5] is not correct. The H/D = 1269.5/908.7 = 1.397 ratio is appropriate for an Nd−H stretching mode. Furthermore, the present HD experiment reveals the three band patterns at 1268.0, 1291.0, and 1313.5 cm^{-1} and at 913.7, 925.7, 937.5 cm^{-1} for the six absorptions of NdH_2D and $NdHD_2$ analogous to those discussed above for the Gd species. Therefore, we are confident that the strong 1269.5 cm^{-1} band is due to the NdH_3 core molecule in solid

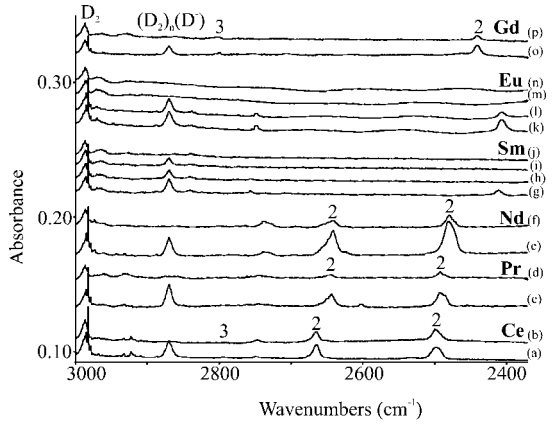

Figure 8. Infrared spectra for the products of reaction of early lanthanide metal atoms with dideuterium during co-condensation at 4 K. (a) Ce codeposition, (b) after >290 nm irradiation; (c) Pr codeposition, (d) after 240−380 nm irradiation; (e) Nd codeposition, (f) after 240−380 nm irradiation; (g) Sm codeposition, (h) after >680 nm irradiation, (i) after 530 nm irradiation, and (j) after 240−380 nm irradiation; (k) Eu codeposition, (l) after >680 nm irradiation, (m) after 240−380 nm irradiation, and (n) after >220 nm irradiation; and (o) Gd codeposition, and (p) after 240−380 nm irradiation.

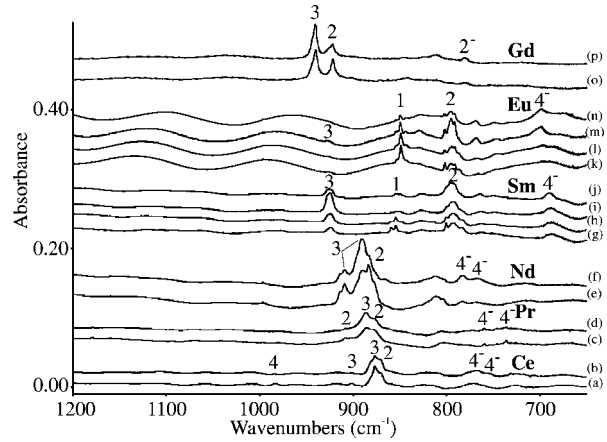

Figure 9. Infrared spectra for the products of reaction of early lanthanide metal atoms with dideuterium during co-condensation at 4 K. (a) Ce codeposition, (b) after >290 nm irradiation; (c) Pr codeposition, (d) after 240−380 nm irradiation; (e) Nd codeposition, (f) after 240−380 nm irradiation; (g) Sm codeposition, (h) after >680 nm irradiation, (i) after 530 nm irradiation, and (j) after 240−380 nm irradiation; (k) Eu codeposition, (l) after >680 nm irradiation, (m) after 240−380 nm irradiation, and (n) after >220 nm irradiation; and (o) Gd codeposition, and (p) after 240−380 nm irradiation.

hydrogen. The weaker band at 1230.2 cm^{-1} is assigned to $NdH_2(H_2)_y$, which is higher than the previous argon matrix assignment to NdH_2.[5] We repeated these argon matrix experiments at 5 K and reaffirm the 1148 cm^{-1} assignment to NdH_2 including HD and D_2 substitution, as discussed by Willson and Andrews.[5]

The 1291.1 cm^{-1} SmH_3 core band is increased five fold on >470 nm visible irradiation, which destroys a sharp 1197.7 cm^{-1} absorption. Our calculations predict a strong 1243 cm^{-1} harmonic fundamental for the octet ground-state SmH, and the sharp 1197.7 cm^{-1} band (H/D ratio 1.402) is appropriate for SmH, of course in the $SmH(H_2)_y$ complex. Next, 240−380 nm ultraviolet irradiation almost removes the 1291.1 cm^{-1} band and restores some of the SmH signal, and subsequent visible irradiation of >530 nm reverses this process (Figure 4g−j). Therefore, the $SmH + H_2 \rightarrow SmH_3$ reaction is reversible with vis−UV irradiation. In addition, the SmH_3 identification is confirmed with mixed H and D species as bands observed at 1291.1, 1311.8, and 1335.5 cm^{-1} and at 927.8, 940.1, and 951.9 cm^{-1} for SmH_2D and $SmHD_2$, as described above for the Gd species. Finally, the 1113.6 cm^{-1} band is assigned to the antisymmetric Sm−H stretching mode in SmH_2, which is lower than the 1156.5 cm^{-1} band so assigned in solid argon[5] owing to complex formation. Our calculated 1194 cm^{-1} fundamental for the septet state SmH_2 and its red shift in complexes are supportive; however, our calculation for SmH_3 finds a planar molecule with 1125, 1175, and 1277 cm^{-1} frequencies. Fortunately, complexation with H_2 tends to increase and coalesce the frequencies (1220, 1239, and 1252 cm^{-1} for the bis complex), so our observation of a strong 1291 cm^{-1} band for $SmH_3(H_2)_y$ in solid hydrogen is reasonable.

The spectra of Sm and Eu in solid deuterium (Figures 8 and 9) reveal new photosensitive D−D stretching bands at 2411 and 2406 cm^{-1} that track with no other bands in these experiments, and the H−H counterparts are too weak to be observed in solid hydrogen. We performed calculations for metal atom complexes with dihydrogen and found reasonable agreement in the case of Sm and Eu, but for all other early lanthanide metals, these calculations do not match the observed bands. In the case of Ce, Pr, Nd, and Gd, the observed H−H stretching modes track with Ln−H stretching absorptions and agree best with the $LnH_2(H_2)_y$ model.

TABLE 4: Bonding Decomposition Scheme for the Lanthanide and Group VI Atoms, Including Uranium[a]

	La	Ce	Pr	Nd	Sm	Eu
prep MH_2	1.0	0.4	0.9	0.5	3.0	0.7
prep $(H_2)_4$	4.5	5.7	4.9	4.7	3.8	3.7
interaction $MH_2-(H_2)_4$	−26.6	−26.9	−20.6	−19.0	−17.3	−13.1
total int energy	−21.2	−20.9	−14.8	−12.9	−10.5	−8.8
	Cr	Mo	W	Nd	U	
prep MH_4	0.0	36.0	24.5	4.1	2.1	
prep $(H_2)_4$	77.4	21.6	24.4	8.0	6.4	
interaction $MH_4-(H_2)_4$	−124.0	−123.9	−118.0	−30.5	−37.8	
total int energy	−46.6	−66.3	−69.1	−18.3	−29.3	

[a] Supermolecule has been decomposed in two fragments, the MH_2 and $(H_2)_4$. In the case of Cr, the decomposition is between Cr and $(H_2)_6$. As mentioned in the text, we could find only a higher energy state for the $NdH_4(H_2)_4$, but for the purpose of analysis, we have used it in the discussion.

In the europium spectrum, the EuH band is very photosensitive, but a clear relationship with EuH_2 is not obvious. The sharp 1189.4 and structured 1112.7 cm^{-1} features are both substantially decreased by >470 nm irradiation, but >380 nm exposure restores some of the latter, whereas continued 240−380 nm irradiation decreases the latter and slightly increases the former absorptions. The sharp 1189.4 cm^{-1} band is assigned here to the ground-state EuH molecule (H/D isotopic frequency ratio 1.402), whereas our calculation finds 1208 cm^{-1} for the nonet ground state. The 1112.7 cm^{-1} feature (H/D ratio 1.400) arises from the antisymmetric EuH stretching mode of the EuH_2 core molecule observed at 1155.6 cm^{-1} in solid argon[5] and is computed here as 1207 cm^{-1}. Again, mixed isotopic data are confirming because the HD experiment gives 1144.1 and 817.5 cm^{-1} bands for the EuHD core molecule and bands at 1114.5 and 799.7 cm^{-1} for EuH_2 and EuD_2 core species from isotopic exchange in the $EuHD(HD)_y$ complexes.

There is a weak 926 cm^{-1} product of the Eu reaction in solid deuterium, which increases upon photolysis with EuD_2 at the

TABLE 5: Natural Population Charges and Natural Electronic Configurations Computed at DFT/BP86/TZVPP Level of Theory for the Lanthanide and Group VI Atoms, Including Uranium, In Different Molecular Fragments[a]

molecular system	La	Ce	Pr	Nd	Sm	Eu	Gd
M	$5d^1 6s^2$	$4f^1 5d^1 6s^2$	$4f^3 5d^0 6s^2$	$4f^4 5d^0 6s^2$	$4f^6 5d^0 6s^2$	$4f^7 5d^0 6s^2$	$4f^7 5d^1 6s^2$
MH_2	$5d^{1.33} 6s^{0.24}$	$4f^{1.3} 5d^{0.60}\ 6s^{0.78}$	$4f^{2.6} 5d^{0.41}\ 6s^{0.69}$	$4f^{3.8} 5d^{0.34}\ 6s^{0.61}$	$4f^{6.0} 5d^{0.24}\ 6s^{0.46}$	$4f^{7.0} 5d^{0.22}\ 6s^{0.49}$	$4f^{7.0} 5d^{0.47}\ 6s^{1.09}$
charge	1.39	1.29	1.29	1.29	1.34	1.33	1.40
$MH_2(H_2)_4$	$5d^{0.95} 6s^{0.15}$	$4f^{1.25} 5d^{0.85} 6s^{0.15}$	$4f^{2.5} 5d^{0.61}\ 6s^{0.16}$	$4f^{3.8} 5d^{0.40}\ 6s^{0.18}$	$4f^{5.9} 5d^{0.33}\ 6s^{0.19}$	$4f^{7.0} 5d^{0.29}\ 6s^{0.19}$	
charge	1.85	1.76	1.71	1.63	1.60	1.58	
	Cr	Mo	W	Nd	U		
M		$4d^5 5s^1$	$5d^4 6s^2$	$4f^4 5d^0 6s^2$	$5f^3 6d^1 7s^2$		
MH_4		$4d^{4.7} 5s^{0.8}$	$5d^{4.5} 6s^{0.8}$	$4f^{3.3} 5d^{0.5}\ 6s^{0.5}$	$5f^{2.4} 6d^{0.6}\ 7s^{0.1}$		
charge		0.56	0.72	1.86	2.91		
$MH_4(H_2)_4$		$4d^{6.7} 5s^{0.5}$	$5d^{4.5} 6s^{0.56}$	$4f^{3.3} 5d^{0.57}\ 6s^{0.21}$	$5f^{2.4} 6d^{0.7}\ 7s^{0.01}$		
charge	−1.71	−1.23	−1.02	1.94	2.91		

[a] Only the major contributions are shown in the table.

TABLE 6: Total Amount of Charge Transferred from the MH_x [$x = 2, 4$] Moiety to the $(H_2)_4$ Fragment in the Supermolecule Computed with a Natural Population Analysis at DFT/BP86/TZVPP Level of Theory

molecular System	La	Ce	Pr	Nd	Sm	Eu	Gd
$MH_2(H_2)_4$	0.52	0.55	0.47	0.38	0.33	0.29	
	Cr	Mo	W	Nd	U		
$MH_4(H_2)_4$		1.14	1.11	0.34	0.50		

expense of EuD (Figure 9). This weak 926 cm^{-1} band with Eu behaves just like the 924 cm^{-1} SmD_3 absorption, and we believe that the 926 cm^{-1} band is due to the EuD_3 core molecule made from the EuD + D_2 reaction. Therefore, $EuD_3(D_2)_y$ is stabilized by lower ZPE relative to the corresponding EuH_3 complex, which is not observed here.

The spectra in Figures 3 and 4 are concluded with GdH_3 discussed above with the addition of the weak H−H stretching mode at 3888 cm^{-1} that is assigned to the $GdH_3(H_2)_y$ complex. This and the counterpart bands at 3894 cm^{-1} for $SmH_3(H_2)_y$ and at 3904 cm^{-1} for $NdH_3(H_2)_y$ show that the trihydrides bind dihydrogen more weakly than the dihydrides, which give rise to more intense H−H stretching modes in the 3400−3600 cm^{-1} region.

In the previous experiments with La and H_2 in excess argon, a new band was observed at 1114 cm^{-1}, which increased upon annealing and upon photolysis. Assignment to the antisymmetric stretching mode in LaH_4^- was substantiated by HD and D_2 substitution and an even stronger band at 1227 cm^{-1} for the corresponding YH_4^- anion.[6,24] An absorption for LaH_4^- was observed at 1102 cm^{-1} in solid neon, which is listed for La in Table 7. Weak bands were observed for the early Ln metal reactions in solid hydrogen in the 970−1100 cm^{-1} region, which also exhibited slight increases upon photolysis and early annealing (Table 7, labeled 4^- in Figure 4). These bands also shifted with solid deuterium as expected for Ln−H/D stretching modes (Figure 9). For example, the two peaks with Ce at 1067 and 1045 cm^{-1} shifted to 766 and 753 cm^{-1} with deuterium (H/D ratios 1.393, 1.388). In addition the bands are better resolved with Pr at 1072 and 1044 cm^{-1} and with Nd at 1091 and 1054 cm^{-1}. Calculations predicted an extremely strong triply degenerate mode for CeH_4^- at 1124 to 1127 cm^{-1} (intensity 1245 km/mol × 3) and likewise for PrH_4^- at about 10 cm^{-1} lower and for SmH_4^- at another 90 cm^{-1} lower, which supports the identification of these bands as tetrahydride anions. The absorptions for Ce, Pr, and Nd reactions were split by the hydrogen matrix into two bands (the Ce product bands are better resolved in *para*-hydrogen and *ortho*-deuterium, Figure S1 in the Supporting Information), but only a single band was observed for Sm and Eu. These molecular anions are probably formed here through H^- capture by the trihydride molecule (reaction exothermic by 70−80 kcal/mol), except in the case of Eu where the reaction probably involves the dihydride, H, and H^-. Note, however, that the EuD_4^- band is substantially

TABLE 7: Infrared Absorptions (cm^{-1}) Observed for Early Lanthanide Metal Atom Reaction Products with Pure Hydrogen (Top List) or Deuterium (Bottom List) at 4 K[a]

La	Ce	Ce(p-H_2)	Pr	Nd	Sm	Eu	Gd	ident
	3801				3894		3888	3
	[3654]				[3704]		[3720]	
3685	3662	3655	3632	3672				2
[3710]	[3613]		[3670]	[3741]				
3409	3409	3401	3398	3380			3385	2
[3520]	[3426]		[3593]	[3538]			[3417]	
	1381	1380						4
	[1346]							
	1262	1264	1302				1327	3
	[1234]		[1241]				[1288]	
	1256	1258						2
	[1250]							
1214	1234	1236	1266	1270	1291		1313	3
[1234]	[1232]		[1236]		[1200]		[1279]	
	1225	1226	1233	1230	1114	1112	1289	2
	[1236]		[1223]	[1205]	[1168]	[1167]	[1249]	
	1108	1108		1149			1201	?
					1198	1189		1
					[1243]	[1208]		
1102	1067	1069	1072	1091			1083[b]	4^-
[1124]	[1125]		[1120]	[1110]	[1020]	[990]	[1079]	
	1045	1042	1044	1054	976	987		4^-
	[1125]		[1114]	[1110]	[1037]	[1003]		
			Deuterated Species					
	2747	2746[c]					2799	3
2681	2664	2660	2643	2642				2
2466	2497	2487	2485	2479			2441	2
					2411	2406		$M(DD)_2$
	983	983						4
	900	902.6					976	3
	893	895.3	909					2
864	876	878.5	887	908.7	924.1	926	939.9	3
	869	871.9	875	883.2	793.5	790.9	921.5	2
		792.5		811			892.6	?
					854.3	848.5		1
783	766	766	760	783			780[b]	4^-
	753	754	737	770	690	699		4^-

[a] Computed vibrational frequencies (cm^{-1}) at DFT/BP86/TZVPP level of theory for all of the species are given in brackets. For simplicity, we give just the frequencies for the supercomplexes with six H_2 molecules for La, Ce, Nd, and Sm and with four H_2 molecules for Eu and Gd. A complete survey of all computed frequencies for all species is given in the Supporting Information. The last column, ident, stands for the number of x hydrogen atoms in the binary MH_x complex. A question mark, ?, means that the number x could not be identified. [b] These bands are assigned to the dihydride anion. [c] This and bands below from Ce and o-D_2 reaction.

stronger than the EuH_4^- absorption (compare the spectra in Figures 8 and 9), and this is in accord with the zero-point stabilization of the deuteriated species and the observation of EuD_3. (See above.) We note that the tetrahydride anion absorptions are relatively stronger in the group III metal reaction systems[6,24] than with the early lanthanide metals. However, the reaction exothermicity is greater and the metal hydride bonds are shorter for the lanthanide tetrahydride anions, which follows the principle of lanthanide contraction. The present definitive identification of SmH and EuH with 1198 and 1189 cm^{-1} fundamentals in solid hydrogen having little matrix interaction provides an experimental basis to support the SmH octet $[(4f^6)(6s)](\sigma, 6s-1s)^2$ and EuH nonet $[(4f^7)(6s)](\sigma, 6s-1s)^2$ ground-state electronic configurations from our DFT calculations, which were predicted earlier by Dolg and Stoll.[25] These solid hydrogen matrix observations may assist in the eventual observation of the gas-phase spectrum. Finally, the single band observed for Gd at 1083 cm^{-1} and that for the deuterium counterpart at 780 cm^{-1} (H/D ratio 1.388) decrease 30% upon UV irradiation, and these bands are appropriate for GdH_2^- and GdD_2^- because our calculations show that the tetrahydride anion disproportionates to the dihydride anion with frequencies in this region.

Bond Analysis. To understand how different metals interact with H and H_2, we have analyzed the stability of various $MH_x(H_2)_y$ [$x = 2, 3, 4$; $y = 1,..., 6$] clusters. Such a stability can be expressed as the difference between the total energy (including ZPE) of the complexes and the energy of their components, namely, MH_x and yH_2. The total interaction energy term can be decomposed in several contributions, as shown in Table 4 and as explained in the Computational and Experimental Methods section. For simplicity, in the analysis, we will consider only the $MH_2(H_2)_4$ supercomplexes for the lanthanide series and the $MH_4(H_2)_4$ complexes for the group VI series and for Nd and U. We decided to focus on the systems with four H_2 molecules because this is the largest number of H_2 that can bind the WH_4 and MoH_4 species. As for the nomenclature, we will use yH_2 to indicate the number of isolated H_2, whereas $(H_2)_y$ is referred to as the y H_2 molecules in the supercomplex.

When forming the $MH_x(H_2)_y$ supercomplex, a substantial charge transfer between MH_x and $(H_2)_y$ occurs. However, to make our model simpler, we assume that the strain energy term includes only the effect of the geometrical distortion. In other words, we assume that MH_x and $(H_2)_y$ have the same electronic configuration in the supercomplex and as isolated species. In such a way, all of the electronic effects are included in the interaction energy term.

In regards to the lanthanide series, we notice that the total interaction energy decreases going from La to Eu, as shown in Table 3. Neither the MH_2 moiety nor the $4H_2$ molecules undergo any major deformation when they form the supercomplex. The effect of putting four H_2 molecules close to each other, as they appear in the supercomplex $MH_2(H_2)_4$, is only a small destabilization that ranges between 4 and 6 kcal/mol. The preparation energy of MH_2 is almost negligible, about 0.5 to 1.0 kcal/mol. The most significant term that explains the trend of total binding energy is the local interaction between MH_2 and $(H_2)_4$. To understand it, in Table 5, we report the natural electronic configurations of the metal atoms in $MH_2(H_2)_4$ and in the isolated MH_2 molecules. In the latter, the hydrogen atoms behave as the electron attractor, and the lanthanide atom behaves as the electron donor. This is the consequence of a depletion of the 6s orbital on the metal that mainly donates its charge to the 1s orbitals on the hydrogen atoms. A further reorganization occurs on the metal with polarization effects within the 6s, 5d, and 4f orbitals. The total charge on the lanthanide elements in MH_2 varies in the range of +1.39 (La) to +1.29 (Ce, Pr, Nd). In the supercomplexes, $MH_2(H_2)_4$, the metal bears an overall larger positive charge than that in the MH_2 species, and the charge variation along the series is also larger: from +1.85 in La to +1.58 in Eu. This means that some charge transfer occurs from the MH_2 moiety to the $(H_2)_4$ fragment and that the heavier the metal the less it participates in this new type of bonding. An inspection of the natural electronic configurations reported in Table 4 helps us to understand this effect. In going from MH_2 to $MH_2(H_2)_4$, the Ce 6s orbital is depleted of about 0.63e, whereas the Eu 6s orbital is depleted of only 0.30e. Part of this charge goes to the 5d orbitals through polarization induced by the H_2 molecules, whereas the remaining charge is back-donated to the empty antibonding orbitals of the H_2. The 4f orbitals are corelike and act as spectators. This trend is further confirmed when we compute the net charge transfer between the two fragments, as summarized in Table 5.

The behavior is different for group VI elements. The inspection of the preparation energy terms reported in Table 3 indicates that both MH_4 and $(H_2)_4$ are strongly deformed with respect to the lanthanide (and also actinide) elements. For MoH_4 and WH_4, the preparation energy is equal to 36.0 and 24.5 kcal/mol, respectively. A similar amount of energy is required as preparation energy for $(H_2)_4$. The interaction energies are strongly stabilizing and about five times larger than those in the lanthanide series. Because of the large deformation of the fragments, the final bonding energy is three times larger than that in the lanthanide case. By looking at the structures (Figure 2), we already notice that the orientation of the four H_2 molecules in $MoH_4(H_2)_4$ and $WH_4(H_2)_4$, is different compared with the orientation in $NdH_4(H_2)_4$ and $UH_4(H_2)_4$. In the Nd/U case, the H_2 molecules are positioned in between two adjacent hydrogen atoms of the MH_4 moiety (Figure 3b), whereas in the Mo/W case, the H_2 molecules are far from the two hydrogen atoms. To understand this difference, we have to inspect the natural electronic configurations reported in Table 5. It is evident that the 4d (5d) orbitals of Mo(W), unlike in the lanthanide case, are involved directly in the bond with the peripheral H_2 molecules. The contribution is fairly large. The 4d (5d) orbitals of Mo(W) go from an occupation of 4.7 (4.5) in $MoH_4(WH_4)$ to 6.7 (6.4) in $MoH_4(H_2)_4(WH_4(H_2)_4)$, indicating the favorable energetic match with the occupied σ bonding orbitals of the peripheral H_2 molecules that act as electron donors. The charge on Mo and W is negative in the supercomplex, −1.23 and −1.02, respectively. The total net transfer between the two fragments is 1.14 for Mo and 1.11 for W, and the charge, unlike in the lanthanide case, floats from the MH_4 moiety to the H_2 molecules. One should also notice a depletion of the 5s (Mo) and 6s (W) shell that probably accounts for a small backdonation to the $(H_2)_4$ fragment and a concomitant polarization to the 4d (Mo) and 5d (W) shells.

In the chromium case, as already mentioned in the Structures and Energetics section, when $4H_2$ molecules are bound to CrH_4, the supercomplex transforms during geometry optimization to $Cr(H_2)_6$. Hence, we performed a bond decomposition by considering Cr as one fragment and $(H_2)_6$ as the other fragment. The results are presented Table 4. The preparation of the Cr atom is null, whereas the $(H_2)_6$ preparation costs about 77.4 kcal/mol, because of a large Pauli repulsion between the neighboring H_2 molecules in the supercomplex. Most of the contribution to the total bonding energy comes from the interaction energy term, 124 kcal/mol, a value attributable to

an electron donation that takes place from the sigma bonding of H_2 to the 3d orbitals of Cr.

In summary, for the lanthanide series when the MH_2 molecule binds hydrogen molecules, the 4f electrons behave like core, the empty 5d orbitals do not have a favorable energetic interaction with the occupied H_2 bonding orbitals, and most of the bonding interaction occurs because the 6s electrons on the metal are partially transferred to the empty orbitals of the $(H_2)_4$ fragment. NdH_4 and UH_4 follow a similar pattern. For the elements of group VI, the behavior is different, and the d orbitals participate in the bond by withdrawing electrons from the $(H_2)_6$ bonding molecular orbitals.

Conclusions

We have presented the results of a combined spectroscopic and computationals study of lanthanide hydrides with the general formula $MH_x(H_2)_y$, where M = La, Ce, Pr, Nd, Sm, Eu, and Gd, $x = 1-4$, $y = 0-6$. Comparative calculations were also performed on the species in which the central metal, M, is Mo, W, and U.

To understand the dihydrogen complexes formed with lanthanide metal hydride molecules, we have first identified the binary MH_x molecule formed in the ablation/deposition process, which becomes the core of the dihydrogen supercomplex, $MH_x(H_2)_y$. Our investigation has shown that the trihydrides bind dihydrogen more weakly than the dihydrides, which give rise to more intense H−H stretching modes in the 3400−3600 cm^{-1} region. We have observed sharp new absorptions for SmH and EuH and broader absorptions for the MH_4^- anions in solid hydrogen.

The result of the analysis of the bond between the lanthanide metal is that when the MH_2 molecule binds several hydrogen molecules the 4f electrons behave like core, the empty 5d orbitals do not have a favorable energetic interaction with the occupied H_2 bonding orbitals, and most of the bonding interaction occurs because the 6s electrons on the metal are partially transferred to the empty orbitals of the $(H_2)_4$ fragment. The NdH_4 and UH_4 species follow a similar pattern. For the group VI metals, Mo and W, the behavior is different, and the d orbitals participate in the bond by withdrawing electrons from the H_2 bonding molecular orbitals.

Acknowledgment. We gratefully acknowledge support for this research from the U.S. National Science Foundation under grant no. CHE03-52487 and the Swiss National Science Foundation (grant no. 200020-120007).

Supporting Information Available: Calculated frequencies and geometrical coordinates for all structures and infrared spectra for Ce reactions with *para*-hydrogen and *ortho*-deuterium. This material is available free of charge via the Internet at http://pubs.acs.org.

References and Notes

(1) Thematic Issue on Hydrogen, *Chem. Rev.* **2007**, *107*, 3899−4435.
(2) Kubas, G. J.; Ryan, R. R.; Swanson, B. I.; Vergamini, P. J.; Wasserman, H. J. *J. Am. Chem. Soc.* **1984**, *106*, 451–452.
(3) Kubas, G. J.; Ryan, R. P.; Wrobleski, D. A. *J. Am. Chem. Soc.* **1986**, *108*, 1339–1341.
(4) Kubas, G. J. In *Modern Inorganic Chemistry*; Fackler, J. P. J., Ed.; Kluwer Academic/Plenum: New York, 2001.
(5) Willson, S. P.; Andrews, L. *J. Phys. Chem. A* **2000**, *104*, 1640–1647.
(6) Wang, X. F.; Chertihin, G. V.; Andrews, L. *J. Phys. Chem. A* **2002**, *106*, 9213–9225.
(7) Wang, X. F.; Andrews, L.; Gagliardi, L. *J. Phys. Chem. A* **2008**, *112*, 1754–1761.
(8) Wang, X. F.; Andrews, L.; Infante, I.; Gagliardi, L. *J. Am. Chem. Soc.* **2008**, *130*, 1972–1978.
(9) Gagliardi, L.; Pyykko, P. *J. Am. Chem. Soc.* **2004**, *126*, 15014–15015.
(10) Raab, J.; Lindh, R. H.; Wang, X. F.; Andrews, L.; Gagliardi, L. *J. Phys. Chem. A* **2007**, *111*, 6383–6387.
(11) Wang, X. F.; Andrews, L. *J. Am. Chem. Soc.* **2002**, *124*, 5636–5637.
(12) Wang, X. F.; Andrews, L. *J. Phys. Chem. A* **2003**, *107*, 570–578.
(13) Wang, X. F.; Andrews, L. *J. Phys. Chem. A* **2005**, *109*, 9021–9027.
(14) Ahlrichs, R.; Bar, M.; Haser, M.; Horn, H.; Kolmel, C. *Chem. Phys. Lett.* **1989**, *162*, 165–169.
(15) Cao, X. Y.; Dolg, M. *J. Chem. Phys.* **2001**, *115*, 7348–7355.
(16) Perdew, J. P.; Burke, K.; Ernzerhof, M. *Phys. Rev. Lett.* **1996**, *77*, 3865–3868.
(17) Ernzerhof, M.; Scuseria, G. E. *J. Chem. Phys.* **1999**, *110*, 5029–5036.
(18) Infante, I.; Gagliardi, L.; Scuseria, G. E. *J. Am. Chem. Soc.* **2008**, *130*, 7459–7465.
(19) Infante, I.; Raab, J.; Lyon, J. T.; Liang, B.; Andrews, L.; Gagliardi, L. *J. Phys. Chem. A* **2007**, *111*, 11966–12000.
(20) Gagliardi, L.; Heaven, M. C.; Krogh, J. W.; Roos, B. O. *J. Am. Chem. Soc.* **2005**, *127*, 86–91.
(21) Andrews, L. *Chem. Soc. Rev.* **2004**, *33*, 123–132.
(22) Silvera, I. F. *Rev. Mod. Phys.* **1980**, *52*, 393–452.
(23) Andrews, L.; Wang, X. F. *Rev. Sci. Instrum.* **2004**, *75*, 3039–3044.
(24) Wang, X. F.; Andrews, L. *J. Phys. Chem. A* **2004**, *108*, 1103–1106.
(25) Dolg, M.; Stoll, H. *Theor. Chim. Acta* **1989**, *75*, 369–387.

JP8099658